Development of microbeads from unmodified biomass with tunable size and competitive mechanical properties

Benjamin Robertson[1], Lena Hoover[2], Gerald Rott[1], Michelle Quan[1] and Michelle Calabrese[1*]

[1*]Department of Chemical Engineering and Materials Science, University of Minnesota, 421 Washington Ave SE, Minneapolis, 55455-0132, Minnesota, United States.
[2]Department of Chemical and Biological Engineering, University of New Mexico, MSC01 1120 1 University of New Mexico, Albuquerque, 87131, New Mexico, United States.

*Corresponding author(s). E-mail(s): mcalab@umn.edu;
Contributing authors: robe2030@umn.edu; lena.hoover@gmail.com; rott0062@umn.edu; quanx065@umn.edu;

Abstract

Despite national and international regulations, plastic microbeads are still widely used in personal care and consumer products (PCCPs) as exfoliants and rheological modifiers, causing significant microplastic pollution following use. As a sustainable alternative, microbeads were produced by extrusion of biomass solutions and precipitation into anti-solvent. Despite using novel blends of biodegradable, non-derivatized biomass including cellulose and Kraft lignin, resulting microbeads are within the shape, size, and stiffness range of commercial plastic microbeads, even without crosslinking. Solution processability and resulting bead shape and Young's modulus can be tuned *via* biomass source, concentration, and degree of polymerization; biomass concentration, extrusion geometry, and precipitation and extraction conditions control the bead size. Lignin incorporation reduces the solution viscosity, which improves processability but also produces flatter beads with higher moduli than cellulose-only microbeads. While some lignin leaches from the beads when stored in water, adding surfactants like sodium dodecyl sulfate suppresses this effect, resulting in good mechanical stability over two months with no noticeable structural degradation. The stability of these mixed-source biomass

microbeads - despite the absence of chemical crosslinking or derivatization - makes this route a promising, robust approach for obtaining environmentally-benign microbeads of tunable size and stiffness for use in PCCPs.

Keywords: lignin, cellulose, biomass, microbeads, biodegradable, mechanical testing

1 Introduction

Plastic microbeads, typically composed of non-degradable synthetic polymers like polyethylene and polypropylene, are used as exfoliants and rheological modifiers in personal care and consumer products (PCCPs) to improve viscosity, bulking, film formation, and abrasion (Leslie, 2014).The quantity of microbeads in PCCPs can be substantial; exfoliating shower gels can contain as much microbead plastic as their packaging (Programme, 2020). Yet unlike the plastic used to package these products, microbeads cannot be readily collected for recycling as they directly enter the water waste stream upon use. While 95-99.9% of microbeads are captured *via* sedimentation during wastewater treatment (Rochman et al, 2015), an estimated 8 billion beads per day enter US aquatic habitats, where they enter the food chain and detrimentally impact aquatic life (Rochman et al, 2015; Parker et al, 2021; Hart and Arlinghaus, 2021).

While fourteen countries have some form of microbead regulations (Xanthos and Walker, 2017), the United States (US) legislation on plastic microbeads which became effective in 2017 is narrow. In applications outside "personal care" and "rinse-off" products categories, including cosmetics, deodorants, and lotions, plastic microbeads are not regulated (Usman et al, 2022; Rochman et al, 2015; McDevitt et al, 2017). In applications where they are not banned, the cosmetic industry continues to employ these microbeads due to their well-defined sizes and shapes, which allow for reliable tuning of flow and abrasive properties as well as facilitating the delivery of active ingredients (Leslie, 2014). While natural scrubs incorporating ingredients like nut shells (Habib et al, 2020), seeds, or mineral abrasives like pumice (Piotrowska et al, 2020) may provide the exfoliating characteristics of plastic microbeads (Nadiratuzzahra and Tristantini, 2020), the rheological properties cannot easily be tuned with these ingredients. Biocompatible microbeads sourced from synthetic polymers are also challenging for PCCP applications. For example, polymers used in drug delivery like poly(D,L-lactide-co-glycolide) (PLGA) degrade too rapidly to be considered in PCCP applications (Mi et al, 2002), and polymers such as polylactic acid (PLA) are unsuitable, as they degrade incompletely in ambient conditions (Rochman et al, 2015; Nam and Park, 2020; Programme, 2020).

Biocompatible and biodegradable microbeads sourced from biomass can provide a sustainable alternative to plastic microbeads currently sourced from synthetic polymers. Microbeads from biomass like cellulose and lignin, which is typically burned or used in low-value products (Graglia et al, 2015), have been previously used for pollutant capture and environmental remediation (Sameni et al, 2018; Beisl et al, 2017; Ge et al, 2016; Mohammed et al, 2018; Omo-Okoro et al, 2018). As

the majority of plastic microbeads in PCCPs are captured during wastewater treatment, these bio-based alternatives may have additional utility after consumer use due to their adsorption and water purification capabilities. Biomass-sourced microbeads are also capable of being produced using industrial equipment (Sameni et al, 2018), and biomass nanoparticles are currently being explored for drug delivery, adhesives, and crop additives (Sameni et al, 2018; Beisl et al, 2017; Mohammed et al, 2018). Unfortunately while synthesis of biomass nanospheres is extremely common, these widely-used processes are limited to producing particles with diameters from nanometers to tens of microns (Beisl et al, 2017; Zhao et al, 2016; Sameni et al, 2018).

Although microbeads are commonly defined as particles ranging in diameter from 0.1 to 5 mm (Canada, 2015; Moore, 2008; Leslie, 2014), particles in commercial PCCPs are anywhere from tens of microns in diameter to over a millimeter (Coombs OBrien et al, 2017; Cheung and Fok, 2017; Fendall and Sewell, 2009; Habib et al, 2020; Napper et al, 2015; Ziajahromi et al, 2017). However, wastewater treatment plants typically use screens and settling tanks to remove microparticles, meaning that particles smaller than ~200 μm may be more likely to escape into the environment (Habib et al, 2020; Ziajahromi et al, 2017; Carr et al, 2016). Beyond this limit, the ideal size of microbeads depends on their intended application - whereas microbeads in toothpaste are usually less than 400 μm (Carr et al, 2016), many microbeads found in skin cleaning products like facial and body scrubs are larger, from 450 to 800 μm (Shareef and Shareef, 2021; Gouin et al, 2015; Duis and Coors, 2016). Larger beads are generally more powerful exfoliants (Shareef and Shareef, 2021), whereas smaller beads may be more suited as rheological modifiers due to the increased colloidal interactions between beads (Macosko, 1994). Consequently, while larger or smaller microbeads could be used as filler particles or as more powerful exfoliants respectively, a reasonable target range for sustainable microbeads in consumer products would be anywhere from 200 to 800 μm in diameter, large enough to be captured in wastewater treatment, and small enough to be used in different personal care consumer products.

As most current processes for synthesizing biomass microbeads produce particles too small for the desired PCCP applications (Beisl et al, 2017; Zhao et al, 2016; Sameni et al, 2018), limited sustainable alternatives to plastic microbeads on the desired size scale relevant to the PCCP industry currently exist (Coombs OBrien et al, 2017; King et al, 2017; Nam and Park, 2020; Volant et al, 2021). Current sustainable alternatives to plastic microbeads utilizing only biomass employ single sources of biomass like cellulose (Coombs OBrien et al, 2017; Xia et al, 2022) and chitin (King et al, 2017; Ju et al, 2021). However, King et al. (King et al, 2017) found that chitin microbeads only formed when the chitin feedstock was extracted from crustaceans, an expensive source that is also a common allergen (Alvarez, 2014); commercial chitin was unsuccessful. Other model systems employed covalent crosslinking to stabilize the microbeads or utilized derivatized biomass (Coombs OBrien et al, 2017; Bai and Li, 2006; Ge et al, 2016; Zhang et al, 2020). Crosslinking and derivatization can both negatively impact enzymatic degradation of microbeads, and certain types of derivatization also result in harmful degradation products (Hamdi and Ponchel, 1999;

Bhattacharjee and Perlin, 1971; Puls et al, 2011; SAPEA, 2019). For instance, Ge et al. (Ge et al, 2016) produced lignin microspheres in the appropriate size range but used only 20% lignin by weight, with the remainder comprised of polyethyleneimine crosslinked with epichlorohydrin. Other systems are not characterized with respect to mechanical stability (King et al, 2017; Ju et al, 2021; Xia et al, 2022) or require highly specific conditions for cellulose dissolution that limit the window for industrial processing (Luo and Zhang, 2010; Luo et al, 2015; Trygg et al, 2013).

Here, we address these challenges by synthesizing a range of microbeads from nonderivatized biomass using low-temperature protocols with low volatility solvents that can be recovered and recycled. Expanding on previous work by Coombs O'Brien et al. (Coombs OBrien et al, 2017) which employs a single biomass source and introduces covalent crosslinking, we utilize this low-energy and versatile synthetic approach to produce and characterize numerous microbead formulations that are mechanically tough without covalent stabilization, investigating the role of lignin incorporation and processing parameters on the resulting properties. *Via* image analysis, scanning electron microscopy (SEM), and single-particle compression testing, we quantify the impact of biomass concentration and composition, cellulose molecular weight, precipitation and extraction solvents, and extrusion geometry on the microbead size, swelling behavior, shape, and stiffness. This straightforward method for producing biomass microbeads is a tunable and robust approach for controlling dimensions and stiffnesses of these beads for use in a range of consumer product applications.

2 Materials and methods

2.1 Materials

Avicel PH-101 (degree of polymerization (DP)=230) and MCC 102 (DP=290) cellulose powders (Sigma-Aldrich) and Kraft dealkaline lignin (TCI Chemical) were used as-received. Ionic liquid (1-ethyl-3-methyl-imidazolium acetate, EMImAc) was purchased from Astatech (95%). Dimethyl sulfoxide (DMSO) was purchased from Oakwood Chemical (ACS-grade). Solvents include acetone (ACS-grade, Fisher), ethanol (100% vol., Pharmco-Aaper), distilled water (HPLC grade, Fisher), and 0.1 M hydrochloric acid (HCl) diluted from concentrated ACS-grade (Macron).

2.2 Biomass solution preparation

Celluloses (DP=290 and DP=230) were dissolved at 8% wt in 70:30 by volume dimethylsulfoxide (DMSO):1-ethyl-3-methylimidazolium acetate (EMImAc) adapted from Coombs O'Brien and coworkers (Coombs OBrien et al, 2017). Cellulose was also dissolved at 7.2 % wt (DP=290), 7% wt (DP=230), 6% wt (DP=230), and 4% wt (DP=230) in the 70:30 DMSO:EMImAc solvent. Cellulose with different DPs were kept separate. Lignin-cellulose solutions were prepared with 8% wt overall biomass and fractions of lignin (f_{lignin}) of 0.33 (2.7 % wt lignin / 5.3 % wt cellulose) and 0.5 (4 % wt lignin / 4% wt cellulose). Solutions were prepared by adding weighed biomass compositions to the 70:30 DMSO:EMImAc solvent and stirring at

40 °C for a minimum of 16 h until all biomass visibly dissolved. Solutions were kept at room temperature until used for microbead preparation.

2.3 Extensional rheology *via* capillary-driven thinning

Capillary-driven thinning extensional rheology measurements were performed using the dripping-onto-substrate (DoS) method as described by Dinic and coworkers (Dinic et al, 2015), using an environmental control chamber as described by Robertson and Calabrese (Robertson and Calabrese, 2022). The primary purpose of this environmental control chamber was to limit water uptake by the hygroscopic ionic liquid solutions during microbead synthesis. Pendant drops of several solutions (8% wt DP290 cellulose, 8% wt DP230 cellulose, and 4% wt DP230 cellulose/4% wt Kraft lignin all in 70:30 DMSO:EMImAc) were brought into contact with glass substrates to form a semi-stable liquid bridge. High-speed videos of the thinning liquid bridges were recorded to determine the minimum radius R over time, using image analysis as described in our prior work (Lauser et al, 2021; Robertson and Calabrese, 2022; Zhang and Calabrese, 2022). Prior to contact with the substrate, the surface tension σ of each solution was measured *via* an ImageJ plugin (Daerr and Mogne, 2016), and subsequently used to determine apparent extensional viscosities η_E, where $\eta_E = \frac{\sigma}{2dR(t)/dt}$. Radial decay profiles were used to determine the Hencky strain, ε_H, where $\varepsilon_H = -ln(R/R_0)$; here, R_0 is the initial radius, defined as 80% of the radius of the nozzle extruding the drop. Radial decay profiles and extensional viscosity as a function of ε_H are shown in SI.3.

2.4 Microbead synthesis & purification

Large batches of beads were synthesized *via* a dripping method adapted from Coombs-O'Brien and coworkers (Coombs OBrien et al, 2017) using a syringe pump and subsequently purified *via* Soxhlet extraction (Fig. 1). Biomass solutions were loaded into syringes with variable nozzle size (30g, 26g, 22g), positioned to be normal to and 7 cm above the surface of the precipitation solvent at which was kept at room temperature (22 ± 1 °C) and ~30% humidity. For all trials except those examining nozzle size (Sec. 3.4), the widest 22g nozzle was used to provide optimal processing conditions. Every ~15 min of dripping, the nozzle was wiped to reduce accumulation of biomass solution on the outside of the nozzle, which could lead to larger drops and larger beads if proceeding unhindered (see Fig. S3). Following precipitation, ionic liquid remaining in the microbead was removed *via* Soxhlet extraction overnight (~12 hours) with 200 mL of the extraction solvent. After extracting using ethanol or water for extraction solvents, microbeads were removed and allowed to air dry overnight (~12 hours). 'Deswelling,' or shrinking of the bead, was visible after extraction due to drying of the solvent. Here, extracted and dried beads were as small as ~40% of the size of the precipitated drops for cellulose beads extracted in ethanol; the degree of deswelling was much lower for beads extracted in water. (SI.2).

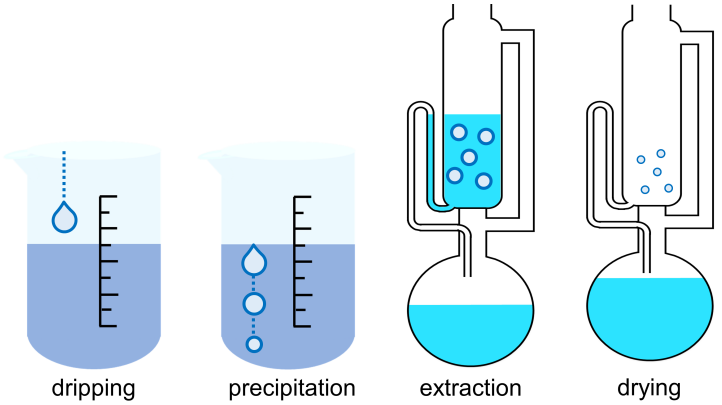

Fig. 1 Schematic of biomass microbead preparation and purification procedure. Biomass solutions were extruded through a nozzle to produce a liquid droplet, which precipitated upon contact with precipitation solvent. Beads were purified *via* Soxhlet extraction to remove residual solvent.

2.5 Precipitation and extraction screen

Precipitation and extraction conditions for the dripping synthesis were determined based on a solvent screen, using the precipitation solvents ethanol, acetone, water, 1:1 ethanol:water (vol.), and 0.1 M HCl. Biomass solutions (8% cellulose, 7.2% cellulose, 2.7 % wt lignin / 5.3 % wt cellulose, and 4 % wt lignin / 4% wt cellulose.) were extruded from a 22g nozzle into these precipitation solvents to produce $n = 5$ beads (with the exception of acetone, for which $n = 1$, and water and ethanol, for which $n = 10$) and to assess differences in size and shape of the beads. Beads precipitated in ethanol and water were each extracted in both ethanol and water, and all other beads were extracted only in ethanol.

2.6 Microbead size quantification

Small batches of beads produced for solvent screen experiments were sized by imaging *via* a Chronos 1.4 high-speed camera with a 10x objective lens and pixel resolution of 1280 by 1024 - each bead was photographed separately. Large batches of beads were placed on white paper and photographed together from above *via* a Samsung Galaxy S9+ phone camera with pixel resolution of 4032 by 3024, with a reference of known size included in each image for calibration. In both cases, images were then analyzed using ImageJ to determine bead sizes, either by manually using the ellipse tool or using a color threshold depending on the quality and contrast of the image. Average diameters D_{bead} were determined based on the area of each ellipse as $D_{bead} = \sqrt{4A/\pi}$, and sphericities were determined based on the ratio of major to minor axes. Many beads ($n \geq 100$ for larger samples, $n = 5$ for smaller samples) were sized to produce a reliable estimate of variance based on sample standard deviation. Swelling ratio was determined as $SR = \frac{D_{wet}}{D_{bead}}$ based on the average size of the extracted and dried beads after being re-swollen in water or SDS solution (D_{wet}) and the average size of the same beads once dried again (D_{bead}). The average bead size prior to extraction and drying (D_{precip}) varied from D_{bead} to $3D_{bead}$ depending on

precipitation and extraction solvents; this decrease in size after extraction and drying was attributed to removal of residual ionic liquid and collapse of the bead pore structure upon evaporation of the extraction solvent (SI.8).

2.7 Scanning electron microscopy (SEM)

Images of microbead surfaces were obtained using a scanning electron microscope (JEOL JSM-6010PLUS/LA). Microbeads were affixed to an adhesive carbon tape without sputter coating. SEM observations were carried out with secondary electron detector at an acceleration voltage of 2 kV to avoid charging effects, with magnifications from 50x to 1000x. Energy-dispersive x-ray spectroscopy (EDS) was performed at an acceleration voltage of 5 kV to ensure sufficient signal (at least 20000 counts per second) for elemental analysis. To determine the microbead internal structure, a microbead was flash-frozen in liquid nitrogen and sectioned with a scalpel.

2.8 Mechanical compression testing

Mechanical single-particle compression testing (Instron, 10kN load cell, see SI.1) was performed by compressing the microbeads at a rate of 0.1 mm per minute. Diameters of individual beads D_{bead} were measured by caliper and confirmed by image analysis prior to compression. The beads were placed on a steel bar which was then placed in between the parallel plates for compression testing. The top plate was lowered within 1 mm of the bead by eye, and bead height H was determined based on the initial gap height (measured by caliper) and the point of contact (as determined by the measured force). Novel bead formulations were tested until fracture or failure (Fig. S10).

To determine Young's modulus, curves of force (F) vs. distance compressed (x) were fit to a Hertzian contact model for the compression of a spheroid between parallel plates (E. Prussia et al, 2006; Rodriguez et al, 1990; Liu et al, 1998; Gao et al, 2021; Portnikov and Kalman, 2014) using Equation 1 where R_C is the bead contact radius (see SI.4) and $E^{'}$ is the apparent Young's modulus:

$$F = \frac{4E^{'}\sqrt{R_C}}{3}x^{3/2} \tag{1}$$

The apparent Young's modulus $E^{'}$ is related to the real Young's modulus of the bead (E) and plates (E_{plate}) *via* Equation 2:

$$\frac{1}{E^{'}} = \frac{1-\nu^2}{E} + \frac{1-\nu_{plate}^2}{E_{plate}} \tag{2}$$

where ν and ν_{plate} are the Poisson ratios of the bead and plates respectively. For $E \ll E_{plate}$, which is true given the high modulus of the steel plates, and small ν ($\nu \sim 0.2$ for measured beads), $E \approx E^{'}$.

The fitting region for the Hertzian contact regime was determined by binning each trial and fitting to Equation 1 within each bin. The linear regime was determined to consist of consecutive bins in which the value of E was statistically equal and did not trend in time. This criterion corresponded visually with the onset of the linear region

of the stress/strain curve indicating complete contact as well as the downturn indicating a plastic response of the material (Portnikov and Kalman, 2014). This fitting region was then fit to Equation 1 to extract a single value of E. Uncertainties from each fit were negligible in comparison to the variation between trials, so uncertainties for average values of E for each sample were calculated as the standard deviation of the fit values for each trial. Statistical significances of differences between moduli were determined *via* a two-sample, one-tailed Student's t-tests (assuming unequal variances).

Due to the effect of contact radius R_C and bead shape in determining E (SI.4), compressive strain ($\varepsilon = x/H$) was plotted vs. force for representative trials following precedent (Coombs OBrien et al, 2017). Force was shown instead of an engineering stress for ease of comparison between beads with different initial areas and shapes, and for more direct assessment of durability under consumer use.

2.9 Stability of microbeads in model systems

Fifty extracted and dried microbeads each with lignin fractions f_{lignin} of 0, 0.33, and 0.5 were re-suspended in water and 25% wt sodium dodecyl sulfate (SDS) in water, for a total of six conditions. Five beads were removed from solution at weekly intervals and dried for 16 hours in a vacuum oven at room temperature, before undergoing mechanical compression tests to assess stability over time. Swelling ratios $SR = \frac{D_{wet}}{D_{bead}}$ were determined based on imaging wet beads immediately after removal from solution and imaging dried beads prior to compression.

2.10 Statistical analysis

All error bars when shown indicate sample standard deviations for at least $n = 5$ trials. Statistical significance was determined *via* a two-sample, one-tailed Student's t-tests (assuming unequal variances), with p-values less than 0.1 considered potentially significant (*), values less than 0.05 considered significant (**), and values less than 0.02 considered very significant (***).

3 Results

3.1 Optimizing microbead precipitation conditions

Precipitation and extraction conditions for the dripping synthesis were determined based on a solvent screen performed on two biomass concentration (8% and 7.2% DP290 cellulose), with the initial screening using the precipitation solvents ethanol, acetone, water, ethanol:water, and 0.1 M HCl (Fig. 2). Microbeads prepared from the same biomass concentration show distinct shapes based on precipitation solvent (Table S1). Acetone was eliminated as a potential precipitation solvent, as its solvent quality for cellulose was too poor to facilitate formation of spherical beads (Fig. 2, column 2). Here, microbeads precipitated immediately upon contact with the solvent, creating a flattened non-spherical shape; as such, no additional screening was performed with acetone. However, the four other ethanol and water-based precipitation solvents were effective in precipitating cellulose microbeads slowly to produce

spherical beads (Fig. 2; see Table S1 for quantification of microbead shapes). However, weak HCl was also removed as a candidate precipitation solvent, as microbeads precipitated in this solvent had a higher propensity for floating near the air-solvent interface rather than settling, leading to irregular shapes for some microbeads.

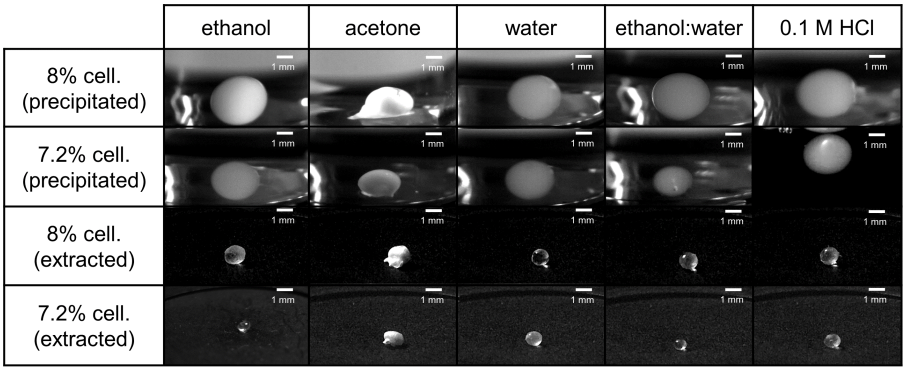

Fig. 2 Images of microbeads produced by extruding solutions of 8% wt and 7.2% wt DP290 cellulose into the given precipitation solvents. All microbeads were subsequently extracted in ethanol. Microbead diameters for all conditions in the solvent screen are listed in SI.2.

Precipitation of cellulose formulations into ethanol, rather than aqueous solvents, generally resulted in formation of beads with smaller average bead diameters, D_{precip}, upon solvent contact (Table S1). These smaller diameters, in addition to supplementary electron microscopy (Fig. S11) and elemental analysis (Fig. SI.8), suggest that ethanol is a more efficient solvent for removing residual ionic liquid than water. One possible explanation is that ethanol has a lower affinity for cellulose which causes microbeads to deswell further and expel ionic liquid more effectively (SI.2), consistent with literature on regenerated cellulose films (Tan et al, 2019). Microbeads both precipitated and extracted in water are more likely to retain non-spherical shapes, due to this residual IL and potentially incomplete water removal (Table S1, SI.8). Accordingly, all microbeads were subsequently extracted in ethanol to efficiently remove residual IL and ensure complete drying of the extraction solvent (Fig. 2). For both cellulose formulations across precipitation solvents, the extraction and drying steps resulted in a statistically significant decrease in microbead size, with the final bead diameter, D_{bead}, around one-half the size of D_{precip} (Table S1). Conversely, no substantial changes in bead diameter were observed between the precipitation and extraction stages when cellulose microbeads were instead extracted with water, suggesting that these beads retain a more porous microstructure. Additionally, these beads contain residual IL and solvent, confirmed by elemental analysis *via* energy-dispersive X-ray spectroscopy (EDS, SI.8).

Interestingly, reducing biomass concentration is a route for reducing bead size, but changing precipitation solvent is not. For example, a 10% reduction in cellulose concentration from 8% to 7.2% wt results in a reduction in the final bead diameter of over 20% for microbeads extracted in ethanol during the solvent screen (Table

S1). However, the microbead size following extraction in ethanol and drying is independent of precipitation solvent for both biomass concentrations (Table S1), despite initial differences in D_{precip}. As the decrease in microbead size upon extraction is due to removal of residual IL and subsequent drying of ethanol which causes the bead to densify, the similarity in D_{bead} following ethanol extraction suggests that nearly all IL is removed, and that all ethanol is dried, regardless of precipitation conditions; this evidence is also consistent with elemental analysis *via* EDS (SI.8). Accordingly, extraction solvent likely impacts the final microbead size more significantly than precipitation solvent.

3.2 Microbead morphology following extraction in ethanol

Scanning electron microscopy (SEM) images of dry microbeads (8% wt DP290 cellulose) following extraction in ethanol reveal a fairly smooth surface morphology (Fig. 3), which is ideal for a use as gentle exfoliants in personal care products (Leslie, 2014). Based on micrographs of the microbead surfaces and additional micrographs of the bead cross-sections (Fig. 3), microbeads precipitated in ethanol appear densely packed, with low porosity on the length scales shown in the images (tens to hundreds of microns). While minor scratches and dimples are observed on the bead surface and in the bulk, no regular pore structure is observed.

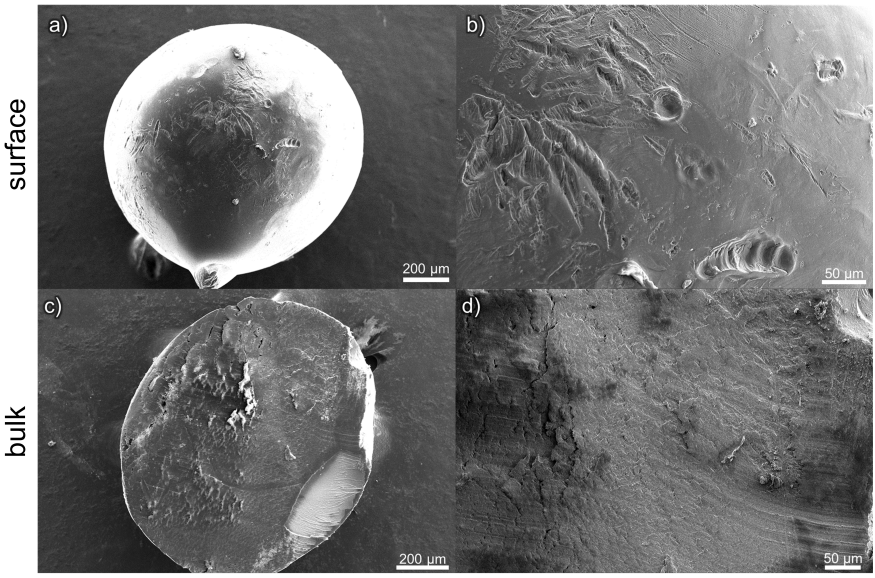

Fig. 3 Surface (a,b) and internal structure (c,d) of microbeads (8% DP290 cellulose precipitated and extracted in ethanol) at a) 70x b) 270x c) 80x and d) 220x magnifications. No visual evidence of a regular pore structure either on the bead surface or in the bulk is observed; only light dimples on the bead surface and microfractures in the bulk (potentially due to sectioning) are observed.

This observation is supported by swelling ratio values near unity for beads extracted with ethanol, indicating that following extraction in ethanol and drying,

cellulose microbeads re-suspended in water are of similar size to extracted and dry microbeads. However, dye adsorption experiments on these cellulose microbeads re-suspended in water (SI.5) suggest a size exclusion phenomenon on ~1 nm length scales, implying a degree of porosity in wet beads on small length scales. These observations for microbeads extracted in ethanol are in contrast to those for microbeads created from the same formulation but precipitated and extracted in water, which had highly porous and fibrous surface morphologies (Fig. S11).

3.3 Impact of precipitation and extraction conditions on mechanical properties

Following the initial solvent screen ($n = 5$), a larger number ($n = 50$) of 8% wt DP290 cellulose microbeads precipitated in either ethanol or water were extracted in either ethanol or water, for a total of four unique precipitation and extraction conditions. Representative images and average properties of microbeads resulting from each condition clearly illustrate the impact of precipitation and extraction solvent on bead diameter, de-swelling (SI.2), and circularity (Fig. 4a, Tables 1, SI.2). Consistent with results from the initial solvent screening, microbeads extracted in ethanol have the smallest diameters, D_{bead} ~1340 μm, with no statistically significant difference in diameter based on precipitation solvent (Table 1). When microbeads are instead precipitated in ethanol and extracted in water, D_{bead} is ~15% larger. As these beads are free of IL (SI.8), this larger bead size could be due to the presence of residual water or due to the slow-drying water preventing a full collapse of the porous microstructure upon drying. However while beads either precipitated or extracted with ethanol remain spherical and relatively small (Fig. 4a), microbeads precipitated and extracted in water are large, soft, and ellipsoidal in shape, reflecting the more porous microstructure and presence of residual fluid.

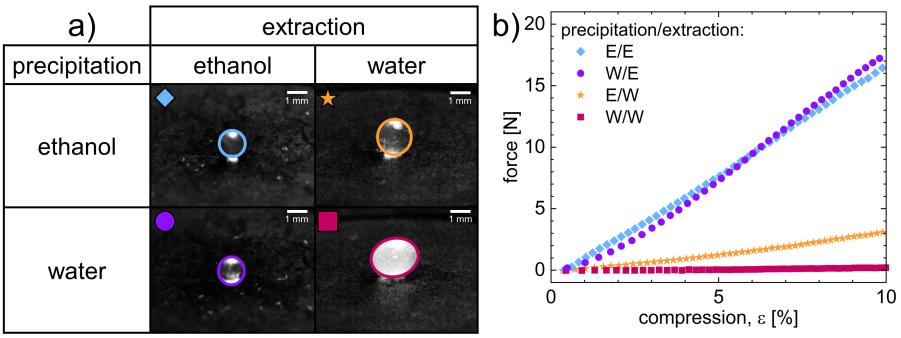

Fig. 4 a) 8% wt DP290 cellulose microbeads with precipitation and extraction solvents of either ethanol or water and b) representative force/compression curves. Beads extracted in ethanol (blue ◆, purple ●, E ~ 0.5 GPa) were one to two orders of magnitude stiffer than beads extracted in water (orange ★, red ■, Table 1). Beads extracted in ethanol had statistically identical Young's moduli ($p = 0.24$), but moduli of all other beads were significantly different (***, $p < 0.02$, SI.13).

Subsequent compression tests on microbeads from each of the four precipitation and extraction conditions confirmed qualitative visual observations, where the Young's moduli of microbeads extracted in water were one to two orders of magnitude lower than for those extracted in ethanol (Fig. 4b, Table 1). Beyond having equal bead diameters, beads extracted in ethanol had statistically identical Young's moduli regardless of precipitation solvent ($E \sim 0.5$ GPa, $p = 0.24$, Table 1). Compression was performed until fracture when possible (Fig. S10); however, microbeads extracted in water did not fracture. As such, all force curves are plotted until 10% compression for ease of comparison (Fig. 4). Conversely, cellulose beads precipitated and extracted in ethanol exhibit a single clean fracture upon break (Fig. S10). The microbead upper surface is also noticeably flattened upon break, leading to a visible radius of contact, as is used in Eqn. 1.

Precipitation	Extraction	E [GPa]	D_{bead} [μm]
Ethanol	Water	0.048 ± 0.014	1544 ± 128
Ethanol	Ethanol	0.479 ± 0.047	1332 ± 82
Water	Water	0.003 ± 0.001	2392 ± 177
Water	Ethanol	0.508 ± 0.076	1345 ± 70

Table 1 Diameters and Young's moduli for microbeads (8% wt DP290 cellulose, 22g nozzle) produced with water and ethanol as precipitation and extraction solvents.

While microbeads extracted in ethanol are significantly stiffer than beads extracted in water regardless of precipitation solvent, beads extracted in water are an order of magnitude stiffer when precipitated in ethanol (Fig. 4b, Table 1). The stiffer beads extracted in ethanol are also substantially smaller than those extracted in water. These results - paired with the identical properties for beads extracted in ethanol - suggest that the softness of beads extracted in water is likely due to their more porous microstructure (Fig. S11) and retention of ionic liquid or solvent serving as a plasticizer (Li et al, 2020; Pang et al, 2013). The identical properties for the beads extracted in ethanol suggest that for those microbeads, residual solvent and IL has been completely removed and that the porous structure has collapsed, leading to a similar degree of de-swelling and thus similar E. Conversely, the varying size, and mechanical properties for beads extracted in water suggest a different degree of IL or solvent retention, an explanation supported by EDS measurements of microbead composition (SI.8). Thus as the change in microbead size and mechanical properties is likely in part due to significant quantities of residual IL, beads precipitated and extracted in water are likely unsuitable for most commercial applications.

3.4 Impact of nozzle size on microbead diameter

While DP290 cellulose formulations produce microbeads with Young's moduli comparable to commercial plastic microbeads (Palombini et al, 2018; Sipe et al, 2022a), these microbeads are challenging to produce *via* dripping synthesis due to the cellulose molecular weight and solution concentration. These properties lead to high solution extensional viscosities, η_E, and weakly elastic behavior in extensional flow (Fig. S2). As such, these solutions can only be extruded through relatively large

nozzles (Fig. S3), limiting the resulting bead size to millimeter scale diameters. To circumvent these challenges and determine if the bead size could be further reduced by adjusting the nozzle size, 7% wt cellulose solutions were examined using a lower cellulose degree of polymerization (DP230, Table 2). Using DP230 cellulose allows several smaller nozzle gauges (22, 26, 30g) to be employed during bead synthesis, as DP230 cellulose solutions have several-fold lower η_E than DP290 solutions, and do not exhibit strain hardening or weakly elastic flow behavior in capillary-driven thinning extensional rheology measurements (SI.3).

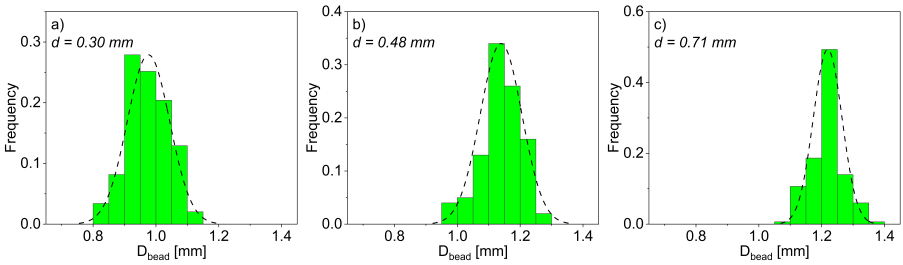

Fig. 5 Diameter size distribution of microbeads (after extraction and drying) formed from 7% wt DP230 cellulose, extruded through nozzles of diameter a) 30 gauge (0.30 mm) b) 26 gauge (0.48 mm) c) 22 gauge (0.71 mm). Mean values and standard deviations determined by fitting a normal distribution (dashed lines) yield: a) 1219 ± 46 μm b) 1139 ± 67 μm and c) 976 ± 67 μm, with $n \geq 100$ for all samples.

Table 2 Diameters for microbeads (7% wt DP230 cellulose, precipitated and extracted in ethanol) produced with 22g, 26g, and 30g nozzles.

Gauge	d [mm]	D_{bead} [μm]
22	0.71	1219 ± 46
26	0.48	1139 ± 67
30	0.30	976 ± 67

Unsurprisingly, smaller nozzles result in smaller bead diameters; however, significantly reducing the nozzle size leads to diminishing returns in terms of reducing D_{bead} (Fig. 5, Table 2). For example, the smallest, 30g nozzle has an outer diameter, d, of 0.30 mm; the dried beads produced from this nozzle have an average D_{bead} of 0.98 mm, which is a 3.2x increase from the nozzle size (Fig. 5c). However, beads produced from the largest, 22g nozzle (d=0.71 mm) have an average D_{bead} of 1.22 mm, an only 1.7x increase in size (Fig. 5a). Thus here, reducing the nozzle size by more than two-fold results in only a 20% reduction in final bead size (Fig. 6). Regardless of nozzle size, microbeads produced from each nozzle exhibit a fairly normal size distribution, with a minimum of D_{bead} ~0.8 mm and D_{bead} ~1.1 mm for the smallest and largest nozzle, respectively.

Differences between D_{bead} and nozzle diameter d result because D_{bead} is determined primarily by the drop size D_{drop}, rather than the nozzle diameter (Fig. 6); D_{drop} is always substantially larger than d. While the nozzle diameter influences the drop

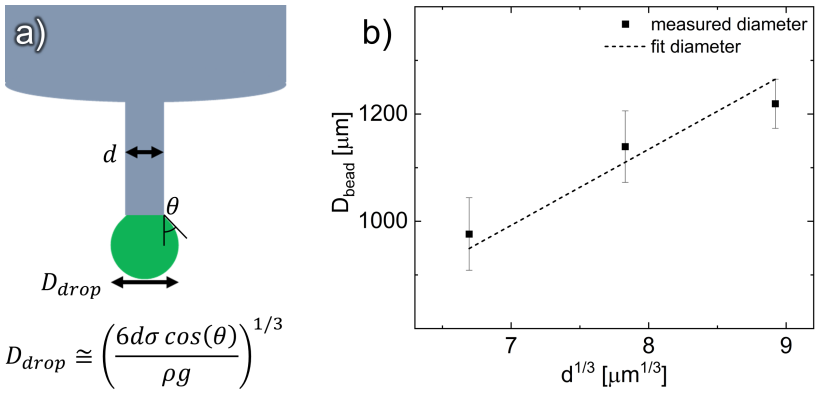

Fig. 6 a) Extruded drop size, D_{drop}, scales with nozzle size d, solution surface tension σ, critical angle θ, and solution surface tension σ and density ρ. b) Bead size D_{bead} also scales with nozzle diameter as $d^{1/3}$ within experimental uncertainty, suggesting that drop size is the primary determinant of bead size for 7% DP230 cellulose solutions.

diameter, D_{drop} is also determined by material properties like surface tension σ, density ρ, and critical angle at breakup θ (Fig. 6). Note that while the drop size is also impacted by the polymer elasticity and extensional relaxation time (Gaillard et al, 2022; Makhnenko et al, 2021), this effect is expected to be small based on the low extrusion flow rate and the absence of strain hardening in DP230 solutions in extensional flow (SI.3). Thus here, drop diameter is expected to scale with nozzle diameter d as $D_{drop} \approx \left(\frac{6d\sigma cos(\theta)}{\rho g}\right)^{1/3}$, based on a balance of surface tension and gravitational forces at breakup (SI.4). In the resulting microbeads, the scaling $D_{bead} \propto d^{1/3}$ fits well within the experimental uncertainty (Fig. 6), suggesting that the ratio of bead diameter D_{bead} to drop diameter D_{drop} remains nearly constant.

3.5 Impact of cellulose concentration on mechanical properties

Given the diminishing returns in reducing bead size by reducing nozzle diameter, reduction of the biomass concentration was pursued next, based on promising solvent screen results showing a significant reduction in D_{bead} from 8% to 7.2% wt cellulose. Given the poor processability of the DP290 cellulose solutions, here DP230 cellulose solutions were formulated at different concentrations (4% to 8% wt). As higher concentration solutions experience high extensional viscosities upon exiting the nozzle (Fig. S2), lower concentration cellulose solutions may provide a route for improving processability *via* increased flow rate through the nozzle.

Visual observations suggest that dilution of the cellulose suspension results in substantially softer beads upon precipitation, likely due to the lower biomass fraction in each initial drop; these differences in bead stiffness persist following extraction (Fig. 7). Here, lowering the cellulose concentration from 8% (green •) to 7% wt (blue □), and again from 7% to 6% wt (yellow ▲) results in microbeads with statistically significant reductions in modulus (***, $p < 0.02$, Fig. 7, Table S12). This reduction in modulus can be seen clearly by the shallower slope in representative force/compression traces with decreasing biomass content (Fig. 7). While the average modulus

of the 4% wt microbeads (red ▽) is lower than that of the 6% formulations, this difference is not statistically significant (*, $p = 0.1$, SI.13). Notably, microbeads formed from 4% solutions exhibit a high degree of variability in both size and mechanical properties (Table 3), leading to the statistical equivalence between the two lowest biomass content solutions; for all raw data, see SI.11. The lower biomass content, especially in the 4% biomass solutions, causes buckling and wrinkling of the surface during extraction and drying as the bead shrinks due to liquid expulsion and rapid collapse of the porous structure (Fig. S5). As a result, 4% microbeads often assume irregular shapes and have surface heterogeneities that lead to high variability in single particle measurements of moduli.

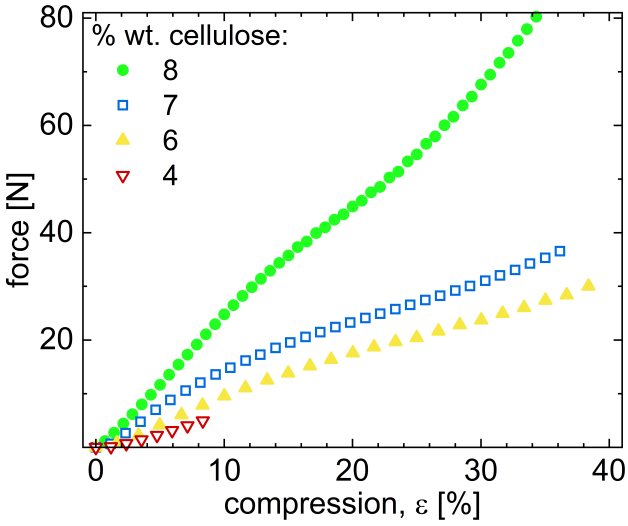

Fig. 7 Representative force/compression curves of 8% (green •), 7% (blue □), 6% (yellow ▲), and 4% (red ▽) wt DP230 cellulose microbeads extracted in ethanol. Bead moduli (Table 3) increased with concentration monotonically, as shown in the force/compression curves. Due to the high variability of the 4% sample, the 4% and 6% samples were statistically similar (*, $p = 0.1$), but moduli of all other samples were significantly different (***, $p < 0.02$, SI.13).

The reductions in modulus with decreasing biomass content are accompanied by reductions in average bead size (Table 3). As with the Young's moduli, these reductions in average bead size are statistically significant when the biomass content is lowered from 8% to 7% and again from 7% to 6% (***, $p < 0.001$ between 8% and 7% and 7% and 6%) as beads shrink more upon extraction with lower initial biomass contents. Possible explanations for the differences in mechanical properties between beads from different biomass concentrations are the formation of microscale voids in the lower concentration beads during the process of precipitation (Schmalbach et al, 2021) or differences in entanglement phenomenon. Additionally, upon anti-solvent contact, cellulose at the droplet surface begins to densify in a region near the surface (see supplemental video), which likely impacts the ultimate mechanical properties of the bead. As lower concentration solutions have a lower density of polymer at the

surface and throughout the drop, the thickness and density of the surface region is expected to differ, likely changing the bead microstructure, especially in the near-surface region, as IL is removed and the bead shrinks.

Cellulose [% wt]	E [GPa]	D_{bead} [μm]
8	0.605 ± 0.023	1287 ± 159
7	0.564 ± 0.020	1219 ± 46
6	0.443 ± 0.020	1092 ± 111
4	0.349 ± 0.137	1102 ± 210

Table 3 Microbead diameter and Young's modulus for formulations using: DP230 cellulose, 22g nozzle, and ethanol as the precipitation and extraction solvent.

Interestingly, the microbeads formed here from DP230 cellulose solutions have higher Young's moduli than for microbeads formed from the analogous solutions prepared with DP290 cellulose, despite the lower molecular weight of the DP230 cellulose; see SI.9 for direct comparison of mechanical compression tests. As direct measurement of molecular weight distributions of cellulose is only possible *via* specialized instruments (Dupont, 2003), the higher moduli in the DP230 microbeads could be due to differences in molecular weight distribution or differences in impurities in the reagent powders. However while the beads are largely amorphous, the higher moduli of the DP230 beads are consistent with higher bead crystallinities measured by XRD (SI.9). Another possible explanation is the lower surface tension of the DP230 bead solutions vs. that of the DP290 solutions (Table S9), indicating that the smaller DP230 cellulose chains are more active at the ionic liquid droplet surface. As cellulose at the droplet surface begins to densify upon anti-solvent contact, the density of DP230 cellulose at the surface of the final microbead may be higher than that for DP290 cellulose, which could result in the higher moduli but lower strains at break observed here (SI.9).

3.6 Tuning microbead properties *via* lignin incorporation

Following extensive characterization of microbeads prepared from cellulose-only solutions, subsequent incorporation of Kraft lignin - a low-value byproduct of the cellulose extraction process (Graglia et al, 2015) - into cellulose solutions demonstrates the robustness of the bead production method to variable feedstocks. Additionally, lignin incorporation provides a potential route for tailoring bead size and stiffness. Lignin addition substantially reduces the extensional viscosity of biomass solutions likely due to its smaller, highly branched structure (SI.3), reducing die swelling and enabling facile and efficient bead production.

3.6.1 Optimizing precipitation conditions

Using the same solvent screen as for pure cellulose microbeads, the optimal precipitation conditions for biomass formulations with increasing quantities of lignin were found to be similar to that of their cellulose-only counterparts. Here, two weight fractions of lignin (f_{lignin}) were substituted into the cellulose to model the properties of

mixed biomass feedstocks, maintaining an overall biomass concentration of 8% with f_{lignin} = 0.33 (2.7% wt lignin / 5.3% wt cellulose solution) and f_{lignin} = 0.5 (4% wt lignin / 4% wt cellulose). As observed for cellulose-only formulations, the solvent quality of acetone is too poor to facilitate formation of spherical beads (Fig. 8); as such, only one bead was precipitated into acetone.

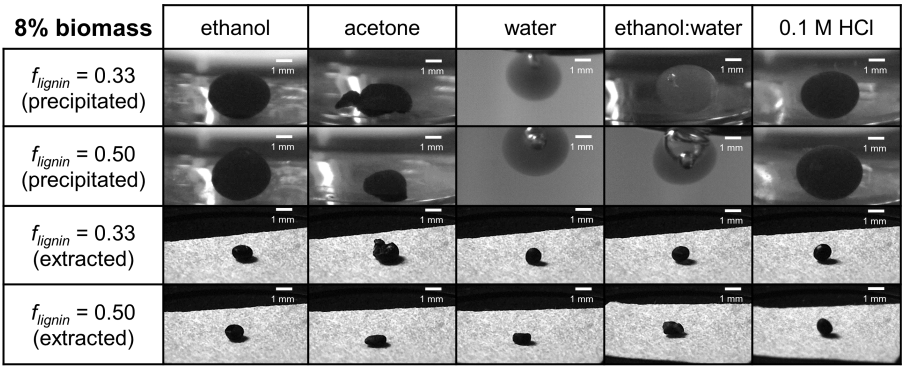

Fig. 8 Images of microbeads produced by extruding solutions (overall 8% wt biomass) of given weight fraction lignin (f_{lignin}) from a 22g nozzle into the given precipitation solvents and extracting in ethanol. Diameters of all microbeads in the second solvent screen are listed in SI.2.

Resulting microbeads exhibit differences in size and shape depending on the precipitation solvent and solution composition; solvent screen results are detailed in SI.2. Lignin-containing solutions generally produce flatter beads, as is evident in the bottom row of Fig. 8 with f_{lignin} = 0.5. Increasing lignin content generally increases the deviation in microbead shape from perfect spheres; however, certain precipitation solvents still produce beads with reasonable sphericities (ratio of major/minor axes ~1.2, Table S1) at 50% lignin content. However, substituting a smaller amount of lignin for cellulose (f_{lignin} = 0.33) is a viable route for creating approximately spherical beads for a number of precipitation conditions. Interestingly, while precipitation and extraction in water produces larger microbeads for cellulose-only formulations, lignin-containing microbeads precipitated and extracted in water are substantially smaller than in all other conditions for both lignin fractions (Table S1).

As opposed to in the solvent screen conducted for pure cellulose compositions, trends in bead size following precipitation and extraction in different solvents for lignin-containing microbeads are more difficult to interpret; these changes in microbead size are complicated by the fact that lignin can diffuse out of the microbead during both processes. For example, discoloration of both the precipitation and extraction solvent occurs for both water and ethanol; however, this effect is substantially more significant in water due to the higher solubility of lignin in water vs. ethanol. Unsurprisingly, lignin-containing beads de-swelled further than their pure cellulose counterparts when extracted in water. Paired with the fact that the smallest beads are produced when precipitation and extraction are in water, lignin leaching likely plays a significant role in determining D_{bead} when water is used for both steps. However across precipitation solvents (Table S1), D_{precip} is significantly smaller for

f_{lignin} = 0.33 than for pure cellulose (p = 0.004) and for f_{lignin} = 0.5 than for f_{lignin} = 0.33 (p = 0.027). This smaller D_{precip} may reflect substantial leaching during precipitation; however, the lower surface tension for lignin-containing solutions should also reduce the initial drop size (Table S9), thus reducing D_{precip}.

Interestingly, precipitating formulations with moderate lignin contents (f_{lignin} = 0.33) into water-containing solvents followed by extraction in ethanol produces the most spherical lignin-containing microbeads (Table S1). These conditions all result in similar microbead sizes, sphericities, and de-swelling ratios ($\frac{D_{bead}}{D_{precip}}$ = 0.5-0.6). These ratios are substantially smaller than for all other conditions, suggesting that both lignin leaching during precipitation in a water-containing solvent and size reduction due to extraction in ethanol must occur. The improved sphericity in these microbeads may reflect that the microbeads become increasingly cellulose-rich as lignin leaches from the bead, leading to enhanced structural reinforcement; conversely, when precipitated and extracted in ethanol, more lignin remains in the microbeads, leading to flattened morphologies. Interestingly, these flattened morphologies occur regardless of precipitation conditions at higher lignin content (f_{lignin} = 0.5), suggesting that a critical content of cellulose may be necessary to retain structural integrity and a highly spherical morphology. Thus while ethanol was used in all large-scale syntheses of lignin-containing beads, these findings suggest that use of water as a precipitation or extraction solvent can provide an opportunity for further tuning the microbead size, shape, and porosity.

3.6.2 Impact of lignin on mechanical properties

Following the solvent screen, larger-scale syntheses of lignin-containing microbeads revealed that the average bead diameter is significantly smaller for lignin-containing microbeads than for those made from pure cellulose (Table 4), though no difference in D_{bead} is observed between f_{lignin} of 0.33 and 0.5. Here, D_{bead} is reported as a spherical average diameter after fitting the microbead cross-sectional areas as ellipses. Notably, this diameter does not account for the flattened morphology in the vertical dimension for lignin-containing beads; thus the similarity in D_{bead} for the two lignin-containing formulations likely does not reflect the true bead volume, which is likely smaller for the highest lignin content microbeads due to lignin leaching.

Cellulose [% wt]	Lignin [% wt]	E [GPa]	D_{bead} [μm]
8	0	0.479 ± 0.047	1332 ± 82
5.33	2.67	0.515 ± 0.036*	1091 ± 71
4	4	0.550 ± 0.038*	1135 ± 126

Table 4 Diameter and Young's moduli for microbeads (8% biomass, DP290 cellulose, precipitated/extracted in ethanol) with f_{lignin}= 0, 0.33, and 0.5. * indicates E calculated using an oblate spheroid model (SI.4) due to the flatter shape and lower curvature at contact for high f_{lignin}.

Lignin-containing beads are flatter and tend to break at lower strains when compressed (Fig. 9); however, their Young's moduli are comparable to those of pure cellulose microbeads (Table 4), suggesting that these microbeads can be a route to valorize this low-value biomass feedstock. In fact, compressing microbeads made

from pure cellulose and those containing up to 50% lignin yields nearly identical force/strain curves up to ~20% compressive strain or around 30 N of normal force (Fig. 9). These data suggest that lignin-containing beads may perform similarly in consumer product applications: while the intensity of scrubbing varies greatly, normal forces applied by the human hand are generally less than 25 N for even strenuous activities (Søgaard et al, 2001), and less than 10 N for gentler activities (Peng et al, 2021; Xu et al, 2019; Xu and Gerling, 2020). Given that the force/strain curves do not account for the smaller cross-sectional area in lignin-containing microbeads, the microbead Young's moduli actually increase with increasing lignin content (Table 4). Differences in E are statistically significant (***, $p < 0.02$) for $f_{lignin} = 0$ and 0.5, but significant to only 90% confidence (*, $p = 0.1$) between 0 and 0.33 and between 0.33 and 0.5 (SI.13). Note that to calculate E, these data are also corrected for the non-spherical bead geometry at high lignin contents; see details in SI.4.

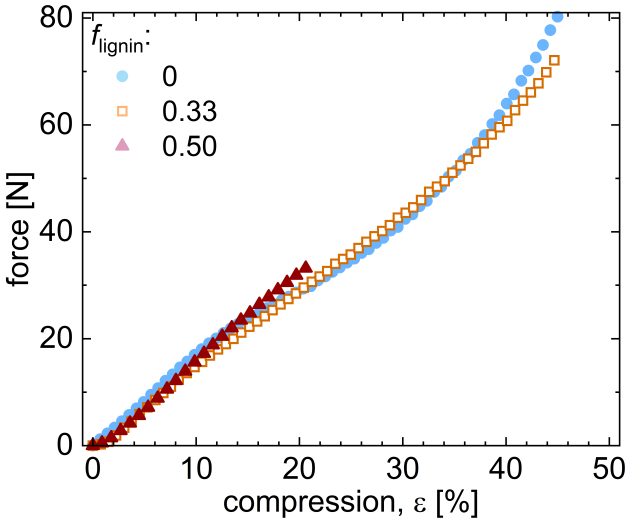

Fig. 9 Representative force/compression curves of 8% (DP290 cellulose) microbeads with f_{lignin} of 0 (blue •), 0.33 (orange □), and 0.5 (red ▲); curves are nearly independent of bead composition at low compressive strains, though higher f_{lignin} beads break at much lower ε. Higher f_{lignin} leads to smaller, flatter beads with higher moduli (Table 4, SI.4).

While microbeads made from pure cellulose or one-third lignin do not break until high compressive strains (>40%), microbeads containing 50% lignin are substantially more brittle, breaking at ~20% strain. These significant differences in compression-at-break for the highest lignin content microbeads likely reflect the flatter morphology in addition to the increased microbead stiffness with increasing lignin content, although even without the morphology adjustments, the smaller average bead contact would led to higher measured moduli for lignin-containing beads. Although beads become stiffer and more brittle with the addition of lignin, even the microbeads with $f_{lignin} = 0.5$ do not break with less than 30 N of force. Additionally, the microbeads precipitated and extracted in ethanol still appear approximately

spherical (Fig. 8) with reasonable sphericities (~1.3), suggesting that even high lignin content microbeads may be commercially-relevant.

3.7 Stability of microbeads in model systems

Two-month stability tests on microbeads submerged in water vs. 25% wt SDS demonstrated that the presence of SDS suppressed diffusion of lignin out of lignin-containing microbeads, illustrated in Fig. 10 for f_{lignin} = 0, 0.33 and 0.5. These differences in diffusion are apparent even at early times (~16 h), where SDS solutions with lignin-containing beads were lighter in color than analogous formulations in water; the solutions darken proportionally to the amount of lignin leached from the microbead. Microbead solutions in water and SDS with cellulose-only beads exhibited no noticeable coloration. Notably, the solution colors after ~16 h (Fig. 10) are similar to those at the end of the two-month stability test (Fig. S7), indicating that the majority of the lignin leaches from the microbead at early times when the initially dry bead re-swells upon contact with the solution. As lignin leaches from the bead more in pure water than in a model SDS solution (Fig. 10a), undesirable lignin leaching could be suppressed upon incorporation of the microbeads into PCCPs. While lignin leaching could potentially be mitigated *via* covalent crosslinking (as performed in lignin-polyethylenimine (PEI) microbeads (Ge et al, 2016)), lignin leaching could also provide a route for producing lower density, more porous microbeads with enhanced suspension stability and sorbent properties (Chern et al, 2004; Ma et al, 2016).

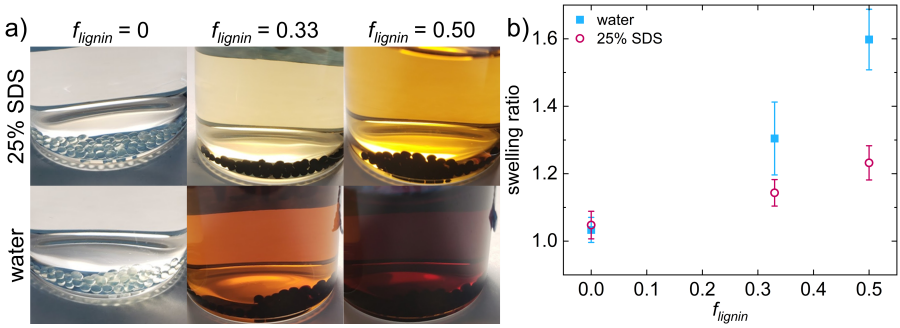

Fig. 10 a) Mixed biomass microbeads (f_{lignin} =0, 0.33, 0.5 with DP290 cellulose) in (top) 25% SDS and (bottom) water after 16 h. SDS mitigates diffusion of lignin from the bead, reflected by the lighter mixture colors. b) Bead swelling ratios SR in water and 25% SDS remain constant over 2 months. (Fig. S8) but increase with lignin content, though this effect is reduced in SDS solutions.

Microbead size measurements taken over the course of the two month stability test indicate no statistically significant change in size over time after initial re-swelling for all six solutions (Fig. 10, SI.6), suggesting that beads maintain good structural stability over this time period. In these stability tests, microbeads were removed from solution each week to understand the impact of the surrounding solution environment on the long-time microbead stability and mechanical properties; for measurement accuracy, beads were thoroughly dried prior to mechanical testing.

For each set of beads, swelling ratios $SR = \frac{D_{wet}}{D_{bead}}$ - which are related to bead porosity (Chern et al, 2004; Ma et al, 2016) - were determined by imaging and sizing wet beads immediately upon removal from solution and following the drying process. For all six solutions, the constant microbead swelling ratios in time indicate good structural stability (Fig. S8). As swelling ratios are related to the pore structure, this finding implies that no significant structural degradation or additional lignin leaching occurs over two months, as both of these events would be expected to alter SR. These data are also consistent with qualitative visual observations that suggest that additional lignin leaching is minimal after the initial re-swelling stage (Figs. 10, S7).

While trends in the swelling ratio are independent of solution condition, average swelling ratios vary in magnitude across conditions and depend on the surrounding medium (water vs. SDS). Microbeads submerged in SDS had consistently lower SR than their counterparts submerged in water, consistent with visual observations that beads submerged in SDS solutions leached less lignin (Fig. 10). For cellulose-only microbeads, average values of $SR \approx 1$ indicate low porosity, and no significant difference in swelling is observed based on surrounding medium ($p = 0.22$). However, lignin leaching - especially from beads suspended in pure water - leads to the recovery of some porosity in wet microbeads, as indicated by swelling ratios. Lignin beads had significantly higher average swelling ratios in water vs. SDS (***, $p < 0.001$ for both pairs), and the average SR increased three-fold faster with f_{lignin} in water than in SDS (Fig. 10).

Submerging beads in lignin vs. SDS also leads to differences in mechanical properties as the beads age. All beads exhibit decreases in compression at break (ε_{break}) and significant increases in moduli (**, $p < 0.05$) of two- to three-fold over time (Fig. S9), pointing to brittleness resulting from increased crystallinity from aging (Graminski, 1970; Zervos, 2010). This change is especially noticeable in ε_{break}, with a large drop after week one for all formulations (SI.6); however promisingly, all formulations maintain compressive strains at break of at least 20% after 2 months. The presence of SDS decreases ε_{break} relative to that obtained in water only for all formulations, an effect which could be attributed to the formation of SDS deposits as the beads are dried before compression - these deposits would have very low mechanical strength, and if formed inside the bead, would cause earlier fracture. After week one, however ε_{break} decreases around 50% faster for beads in water as for beads in SDS (Table S8). Unfortunately, clear differences in moduli in time for formulations in water vs. SDS are not discernible, likely due to high variability between small samples (n=5) measured each week.

4 Discussion

By altering the cellulose-to-lignin ratio and changing processing parameters like overall biomass concentration, nozzle gauge, and precipitation and extraction solvent strength, mechanically robust biomass microbeads of tunable modulus (MPa to ~1 GPa), size (D_{bead} = 800-2000 μm), and swelling ratio (1 - 1.6) could be achieved without the need for covalent crosslinking. Importantly, these microbeads exhibit good mechanical stability over two months whether submerged in water or SDS,

maintaining moduli and compressive strains-at-break reasonable for PCCP applications (Palombini et al, 2018; Sipe et al, 2022a; Søgaard et al, 2001; Peng et al, 2021; Xu et al, 2019; Xu and Gerling, 2020). Notably, PCCPs should have a shelf life around 1-2 years (Diven et al, 2015; Baranova et al, 2014), and microbeads measured here would likely become stiffer and more brittle over time (Zervos, 2010). However, an increase in modulus could actually be beneficial, bringing the properties of these beads closer to some commodity plastics (Sipe et al, 2022b). Additionally, under the forces used by consumers, some decrease in compressive strain at break is possible while retaining the efficacy of these beads during use.

While crosslinking can further increase mechanical properties like the Young's modulus and can potentially mitigate effects from aging, this additional synthetic step would likely negate many of the advantages associated with use of these biomass microbeads. For example, the potentially improved stability imparted by crosslinking would almost certainly reduce microbead degradability in the environment following use (Hamdi and Ponchel, 1999; Bhattacharjee and Perlin, 1971). Additionally, synthetic modification can result in harmful degradation products (SAPEA, 2019), and may change how the microbeads are classified from a regulatory perspective, potentially making them less desirable for industrial adoption. Finally, this chemical modification step would likely hinder scalability due to additional equipment needs and increased process complexity. However as is, the microbeads produced herein can be sustainably sourced and readily biodegradable due to their composition of non-derivatized biomass, providing a greener alternative to a major source of current microplastic pollution.

Despite the broad range of accessible properties, some of the microbeads formulations had undesirable properties for actual consumer use. For example, beads around 2000 μm in diameter and with moduli of several MPa resulted in beads that showed evidence of residual IL, which may make them unsafe for use in consumer products. Likewise, smaller beads produced from lower biomass concentrations were more brittle and more often wrinkled or misshapen (Fig. S5), making them worse candidates for consumer use - although these minor imperfections in surface morphology and shape may be unrecognizable by the consumer once incorporated into a PCCP. Accordingly, the practical size range of microbeads produced with this method was ~800-1300 μm, giving Young's moduli of order 0.5 GPa - on par with the size and moduli of beads resulting from commonly-used synthetic plastics (Palombini et al, 2018; Sipe et al, 2022a). Interestingly, incorporating lignin, a waste product from cellulose production, altered the microbead brittleness, size, and shape to a degree - but in general, similar Young's moduli and bead sizes were obtained regardless of biomass composition. This finding is promising for potential industrial adoption, signalling both that lignin can be used as a low-cost constituent of the microbeads and that the microbead preparation method and resulting properties are fairly robust to biomass source. As lignin tends to leach from the microbeads in water-based media, lignin can also potentially be used as a sacrificial filler molecule to generate more porous beads.

While some of these microbeads meet the high end of the target size range for PCCP applications (Habib et al, 2020; Cheung and Fok, 2017; Shareef and Shareef,

2021; Gouin et al, 2015; Duis and Coors, 2016; Ziajahromi et al, 2017), bead sizes that span the entire target range (200-800 μm) could not be produced due to limitations of the production method. The adaptation of this work to other production methods, like an emulsion-precipitation synthesis (Jo et al, 2019; Coombs OBrien et al, 2017; Volant et al, 2021; Park et al, 2020b,a), would both afford access to smaller bead sizes and enable better scalability using large batch reactors. While dripping methods can be accelerated to commercial scale *via* parallelization or additional apparatus like jet-cutting (Druel et al, 2018), batch reactor mixing is far cheaper to implement, and the supporting infrastructure largely already exists. Furthermore, due to the limitations of the high-viscosity solutions used, an emulsion route is necessary to access beads with diameters within the smaller end of the target range, on the order of 200-700 μm (Habib et al, 2020; Cheung and Fok, 2017; Ziajahromi et al, 2017; Carr et al, 2016). Although previous work by Park and coworkers (Park et al, 2020b) incorporates other biopolymers like lignin into emulsion-based microbeads, the resulting microbeads are too small for use in most PCCPs (Palombini et al, 2018; Kalčíková et al, 2017; Yurtsever and Yurtsever, 2019; Nam and Park, 2020).

Finally, beyond the mismatch in microbead size for the intended PCCP applications, the microbeads examined by Park et al. (Park et al, 2020b) were also too small to perform traditional mechanical compression testing methods. In fact, the size of microbeads produced herein is near the lower limit of what can be measured with a standard single-particle bulk compression testing apparatus. Thus in addition to the numerous PCCP applications requiring larger bead sizes (Fendall and Sewell, 2009; Hintersteiner et al, 2015), the beads produced here also serve as a model system for assessing trends in bead size, bead shape, and mechanical properties *via* more straightforward imaging and mechanical testing methods. This insight can now guide the formulation of smaller beads with tunable properties *via* other methods such as the aforementioned emulsion-precipitation syntheses (Jo et al, 2019; Coombs OBrien et al, 2017; Volant et al, 2021; Park et al, 2020b,a).

5 Conclusion

In this work, biomass microbeads with tunable size, swelling behavior, and mechanical properties were prepared *via* extrusion of biomass solutions, altering both formulation parameters like biomass composition and concentration, and processing parameters including nozzle gauge, precipitation solvent, and extraction solvent. Resulting microbeads have properties on par with those of synthetic plastic microbeads, with moduli ranging from several MPa to nearly 1 GPa, diameters from ~800-2000 μm, and swelling ratios from 1 to 1.6. To our knowledge, this is the first demonstration of microbeads for PCCPs composed of purely biomass which incorporate multiple biomass sources and are highly stable despite the absence of chemical crosslinking or modification. While all microbeads exhibit good structural stability when submerged in water for over 2 months, cellulose microbeads with added Kraft lignin did experience moderate lignin leaching from the bead into the surrounding water. However, use of a sodium dodecyl sulfate solution as a model personal care product leads to high retention of lignin within the microbead structure

despite the absence of crosslinking, a result which is promising for consumer product applications.

Precipitation solvent, biomass concentration, and Kraft lignin fraction substantially impact the resulting microbead shape. Numerous precipitation solvents produce spherical beads; however, lower biomass content leads to nonuniformities in shape, likely due to contraction of the bead surface during precipitation and extraction. Incorporating larger amounts of Kraft lignin leads to flattening of microbeads upon contact with the precipitation solvent, potentially due to a reduction in sample viscosity. While the highly irregular particle shapes produced using acetone as an precipitation solvent preclude its further use, formulations like lignin-containing beads that exhibit smaller deviations from the ideal spherical morphology may still be useful in commercial products.

Incorporating lignin, altering biomass concentration, and using celluloses with different degrees of polymerization provides routes to tune the microbead size, as these factors all impact solution viscosity. Beyond reducing the bead size individually, higher lignin content, lower biomass concentration, and shorter cellulose all result in solutions with lower viscosities that can be extruded through smaller nozzles to produce even smaller beads. However, drastically reducing the nozzle size yields diminishing returns, as the final bead diameter scales with nozzle size, d, as $d^{1/3}$.

The most effective route for tuning the microbead Young's modulus is by altering the extraction solvent, with the initial precipitation solvent playing a minor role. However, large changes in modulus due to extraction solvent result from a more porous microstructure and residual ionic liquid, which is impractical for use in PCCPs. Other routes for tuning the modulus include altering the concentration of biomass and lignin incorporation - of these, altering the biomass concentration may be the most effective, but the high solution viscosities restrict the potential concentration range using the current method. Incorporating lignin, on the other hand, increases the modulus without significantly impacting the force/compression response for compressive strains up to 20%.

While the aforementioned experimental constraints limit the dripping method of microbead production to beads at the upper end of the commercially-relevant size range, successful incorporation of both cellulose and lignin clearly demonstrates the robustness of the method to biomass source. While lignin incorporation does impact the microbead brittleness, size, and shape, remarkably similar ranges of Young's moduli and bead sizes can be obtained regardless of biomass composition. This work thus presents the first demonstration of stable, non-crosslinked biomass microbeads at the PCCP-relevant length scale that incorporate multiple biomass sources, and establishes guidelines for tuning the resulting microbead size, shape, and mechanical properties *via* formulation and processing parameters. These guidelines can then be extended to alternative synthetic approaches that afford access to a wider range of microbead sizes, greatly expanding the number of PCCP applications that can be pursued.

Supplementary information. The Supporting Information includes tables summarizing all solvent screen data; raw data from mechanical testing and dripping-onto-substrate extensional rheometry; additional SEM images, calculations, and stability

test data; dye adsorption experiments; X-ray diffraction; and energy-dispersive X-ray spectra.

Ethics approval and consent to participate. Not applicable

Consent for publication. All authors have provided consent for publication of this manuscript

Availability of data and materials. Any data relevant to this study which are not given in the article or supplementary information are available upon request.

Competing interests. The authors have no relevant competing interests to declare.

Funding. The authors acknowledge the support of the National Science Foundation Center for Sustainable Polymers under Grant No. CHE-1901635. The authors thank the Michael H. Baker Foundation for their support of this project.

Author contributions. B.P.R., J.E.R., and L.M.H synthesized microbeads and performed sizing experiments. B.P.R. and L.M.H. performed compression tests. L.M.H. performed precipitation screen and dye absorption experiments. M.Q performed XRD experiments. B.P.R. performed all other experiments. B.P.R. analyzed data with assistance from M.A.C. B.P.R. and M.A.C. wrote the manuscript. All authors reviewed the manuscript.

Acknowledgments. The authors thank Dr. Michael Manno for training and use of the Valspar Materials Science and Engineering Laboratory for SEM, XRD, and compression testing.

Author contributions. Not applicable

References

Alvarez FJ (2014) The Effect of Chitin Size, Shape, Source and Purification Method on Immune Recognition. Molecules 19(4):4433–4451. https://doi.org/10.3390/molecules19044433

Bai YX, Li YF (2006) Preparation and characterization of crosslinked porous cellulose beads. Carbohydr Polym 64(3):402–407. https://doi.org/10.1016/j.carbpol.2005.12.009

Baranova II, Zhuk OV, Kovtun YV (2014) Determination of the shelf-life and storage conditions for an antimicrobial foam cleanser. News of Pharmacy (1):12–16. https://doi.org/10.24959/nphj.14.1945

Beisl S, Miltner A, Friedl A (2017) Lignin from micro-to nanosize: production methods. Int J Mol Sci 18(6):1244

Bhattacharjee SS, Perlin AS (1971) Enzymatic degradation of carboxymethylcellulose and other cellulose derivatives. J Polym Sci, Part C: Polym Symp 36(1). https://doi.org/10.1002/polc.5070360138

Canada EaCC (2015) Microbeads—A Science Summary. Environment and Climate Change Canada

Carr SA, Liu J, Tesoro AG (2016) Transport and fate of microplastic particles in wastewater treatment plants. Water Res 91:174–182. https://doi.org/10.1016/j.watres.2016.01.002

Chern JM, Lee WF, Hsieh MY (2004) Preparation and swelling characterization of poly (n-isopropylacrylamide)-based porous hydrogels. J Appl Polym Sci 92(6):3651–3658. https://doi.org/10.1002/app.20301

Cheung PK, Fok L (2017) Characterisation of plastic microbeads in facial scrubs and their estimated emissions in Mainland China. Water Res 122:53–61. https://doi.org/10.1016/j.watres.2017.05.053

Coombs OBrien J, Torrente-Murciano L, Mattia D, et al (2017) Continuous Production of Cellulose Microbeads via Membrane Emulsification. ACS Sustain Chem Eng 5(7):5931–5939. https://doi.org/10.1021/acssuschemeng.7b00662

Daerr A, Mogne A (2016) Pendent_drop: An ImageJ Plugin to Measure the Surface Tension from an Image of a Pendent Drop. J Open Res Softw 4(1):e3. https://doi.org/10.5334/jors.97, URL http://openresearchsoftware.metajnl.com/articles/10.5334/jors.97/

Dinic J, Zhang Y, Jimenez LN, et al (2015) Extensional Relaxation Times of Dilute, Aqueous Polymer Solutions. ACS Macro Lett 4(7):804–808. https://doi.org/10.1021/acsmacrolett.5b00393

Diven DG, Bartenstein DW, Carroll DR (2015) Extending shelf life just makes sense. Mayo Clinic Proceedings 90(11):1471–1474. https://doi.org/10.1016/j.mayocp.2015.08.007

Druel L, Niemeyer P, Milow B, et al (2018) Rheology of cellulose-[DBNH][CO 2 Et] solutions and shaping into aerogel beads. Green Chem 20(17):3993–4002. https://doi.org/10.1039/C8GC01189C

Duis K, Coors A (2016) Microplastics in the aquatic and terrestrial environment: sources (with a specific focus on personal care products), fate and effects. Environ Sci Eur 28(1):2. https://doi.org/10.1186/s12302-015-0069-y

Dupont AL (2003) Cellulose in lithium chloride/N,N-dimethylacetamide, optimisation of a dissolution method using paper substrates and stability of the solutions. Polymer 44(15):4117–4126. https://doi.org/10.1016/S0032-3861(03)00398-7

E. Prussia S, K. Tetteh M, P. Verma B, et al (2006) Apparent modulus of elasticity from FIRMTECH 2 firmness measurements of blueberries. Trans ASABE 49(1):113–121. https://doi.org/10.13031/2013.20219

Fendall LS, Sewell MA (2009) Contributing to marine pollution by washing your face: Microplastics in facial cleansers. Mar Pollut Bull 58(8):1225–1228. https://doi.org/10.1016/j.marpolbul.2009.04.025

Gaillard A, Sijs R, Bonn D (2022) What determines the drop size in sprays of polymer solutions? J Non-Newton Fluid Mech 305:104,813

Gao Y, Chai NKK, Garakani N, et al (2021) Scaling laws to predict humidity-induced swelling and stiffness in hydrogels. Soft Matter 17(43):9893–9900. https://doi.org/10.1039/D1SM01186C

Ge Y, Qin L, Li Z (2016) Lignin microspheres: An effective and recyclable natural polymer-based adsorbent for lead ion removal. Mater Des 95:141–147

Gouin T, Avalos J, Brunning I, et al (2015) Use of micro-plastic beads in cosmetic products in Europe and their estimated emissions to the North Sea environment. SOFW-J 141(4):40–46

Graglia M, Kanna N, Esposito D (2015) Lignin Refinery: Towards the Preparation of Renewable Aromatic Building Blocks. ChemBioEng Rev 2(6):377–392. https://doi.org/10.1002/cben.201500019

Graminski EL (1970) The stress-strain behavior of accelerated and naturally aged papers. Tappi J 53(3):406–410

Habib RZ, Salim Abdoon MM, Al Meqbaali RM, et al (2020) Analysis of microbeads in cosmetic products in the United Arab Emirates. Environ Pollut 258:113,831. https://doi.org/10.1016/j.envpol.2019.113831

Hamdi G, Ponchel G (1999) Enzymatic Degradation of Epichlorohydrin Crosslinked Starch Microspheres by α-Amylase. Pharm Res 16(6):867–875. https://doi.org/10.1023/A:1018878120100

Hart PJ, Arlinghaus R (2021) Plastic pollution in rivers and lakes—An indicator of an even bigger consequence of global change? Fish Fish 22(3):465–466. https://doi.org/10.1111/faf.12557

Hintersteiner I, Himmelsbach M, Buchberger WW (2015) Characterization and quantitation of polyolefin microplastics in personal-care products using high-temperature gel-permeation chromatography. Anal Bioanal Chem 407(4):1253–1259. https://doi.org/10.1007/s00216-014-8318-2

Jo S, Park S, Oh Y, et al (2019) Development of Cellulose Hydrogel Microspheres for Lipase Immobilization. Biotechnol Bioprocess Eng 24(1):145–154. https://doi.org/10.1007/s12257-018-0335-0

Ju S, Shin G, Lee M, et al (2021) Biodegradable chito-beads replacing non-biodegradable microplastics for cosmetics. Green Chem 23(18):6953–6965. https://doi.org/10.1039/D1GC01588E

Kalčíková G, Alič B, Skalar T, et al (2017) Wastewater treatment plant effluents as source of cosmetic polyethylene microbeads to freshwater. Chemosphere 188:25–31. https://doi.org/10.1016/j.chemosphere.2017.08.131

King CA, Shamshina JL, Zavgorodnya O, et al (2017) Porous chitin microbeads for more sustainable cosmetics. ACS Sustain Chem Eng 5(12):11,660–11,667

Lauser KT, Rueter AL, Calabrese MA (2021) Small-volume extensional rheology of concentrated protein and protein-excipient solutions. Soft Matter 17(42):9624–9635

Leslie HA (2014) Review of microplastics in cosmetics. IVM Institute for Environmental Studies 476:1–33

Li L, Zhang Y, Sun Y, et al (2020) Manufacturing pure cellulose films by recycling ionic liquids as plasticizers. Green Chemistry 22(12):3835–3841. https://doi.org/10.1039/D0GC00046A

Liu KK, Williams DR, Briscoe BJ (1998) The large deformation of a single micro-elastomeric sphere. J Phys D: Appl Phys 31(3):294–303. https://doi.org/10.1088/0022-3727/31/3/008

Luo X, Zhang L (2010) Creation of regenerated cellulose microspheres with diameter ranging from micron to millimeter for chromatography applications. J Chromatogr A 1217(38):5922–5929. https://doi.org/10.1016/j.chroma.2010.07.026

Luo X, Zeng J, Liu S, et al (2015) An effective and recyclable adsorbent for the removal of heavy metal ions from aqueous system: Magnetic chitosan/cellulose microspheres. Bioresour Technol 194:403–406. https://doi.org/10.1016/j.biortech.2015.07.044

Ma Y, Sun Y, Fu Y, et al (2016) Swelling behaviors of porous lignin based poly (acrylic acid). Chemosphere 163:610–619. https://doi.org/10.1016/j.chemosphere.2016.08.035

Macosko CW (1994) Rheology principles, measurements, and applications. VCH Publishers

Makhnenko I, Alonzi ER, Fredericks SA, et al (2021) A review of liquid sheet breakup: Perspectives from agricultural sprays. J Aerosol Sci 157:105,805

McDevitt JP, Criddle CS, Morse M, et al (2017) Addressing the Issue of Microplastics in the Wake of the Microbead-Free Waters Act—A New Standard Can

Facilitate Improved Policy. Environ Sci Tech 51(12):6611–6617. https://doi.org/10.1021/acs.est.6b05812

Mi FL, Lin YM, Wu YB, et al (2002) Chitin/plga blend microspheres as a biodegradable drug-delivery system: phase-separation, degradation and release behavior. Biomaterials 23(15):3257–3267

Mohammed N, Grishkewich N, Tam KC (2018) Cellulose nanomaterials: promising sustainable nanomaterials for application in water/wastewater treatment processes. Environ Sci Nano 5(3):623–658. https://doi.org/10.1039/C7EN01029J

Moore CJ (2008) Synthetic polymers in the marine environment: A rapidly increasing, long-term threat. Environ Res 108(2):131–139. https://doi.org/10.1016/j.envres.2008.07.025

Nadiratuzzahra S, Tristantini D (2020) Cellulose acetate from oil palm empty fruit bunches waste as biodegradable microbeads for making scrubs. In: AIP Conference Proceedings, vol 2223. AIP Publishing LLC, p 050001

Nam HC, Park WH (2020) Aliphatic Polyester-Based Biodegradable Microbeads for Sustainable Cosmetics. ACS Biomater Sci Eng 6(4):2440–2449. https://doi.org/10.1021/acsbiomaterials.0c00017

Napper IE, Bakir A, Rowland SJ, et al (2015) Characterisation, quantity and sorptive properties of microplastics extracted from cosmetics. Mar Pollut Bull 99(1-2):178–185

Omo-Okoro PN, Daso AP, Okonkwo JO (2018) A review of the application of agricultural wastes as precursor materials for the adsorption of per-and polyfluoroalkyl substances: a focus on current approaches and methodologies. Environ Technol Innov 9:100–114

Palombini FL, Demori R, Cidade MK, et al (2018) Occurrence and recovery of small-sized plastic debris from a Brazilian beach: characterization, recycling, and mechanical analysis. Environ Sci Pollut Res 25(26):26,218–26,227. https://doi.org/10.1007/s11356-018-2678-7

Pang J, Liu X, Zhang X, et al (2013) Fabrication of cellulose film with enhanced mechanical properties in ionic liquid 1-allyl-3-methylimidaxolium chloride (AmimCl). Materials 6(4):1270–1284. https://doi.org/10.3390/ma6041270

Park S, Oh Y, Jung D, et al (2020a) Effect of Cellulose Solvents on the Characteristics of Cellulose/Fe_2O_3 Hydrogel Microspheres as Enzyme Supports. Polymers 12(9):1869. https://doi.org/10.3390/polym12091869

Park S, Oh Y, Yun J, et al (2020b) Cellulose/biopolymer/Fe3O4 hydrogel microbeads for dye and protein adsorption. Cellulose 27(5):2757–2773. https://doi.org/10.

1007/s10570-020-02974-5

Parker B, Andreou D, Green ID, et al (2021) Microplastics in freshwater fishes: Occurrence, impacts and future perspectives. Fish Fish 22(3):467–488. https://doi.org/10.1111/faf.12528

Peng Y, Serfass CM, Kawazoe A, et al (2021) Elastohydrodynamic friction of robotic and human fingers on soft micropatterned substrates. Nat Mater 20(12):1707–1711. https://doi.org/10.1038/s41563-021-00990-9

Piotrowska A, Czerwińska-Ledwig O, Serdiuk M, et al (2020) Composition of scrub-type cosmetics from the perspective of product ecology and microplastic content. Toxicol Environ Health Sci 12(1):75–81. https://doi.org/10.1007/s13530-020-00051-9

Portnikov D, Kalman H (2014) Determination of elastic properties of particles using single particle compression test. Powder Technol 268:244–252. https://doi.org/10.1016/j.powtec.2014.08.011

Programme UNE (2020) Plastics in cosmetics: Are we polluting the environment through our personal care (factsheet). United Nations URL https://wedocs.unep.org/handle/20.500.11822/21754

Puls J, Wilson SA, Hölter D (2011) Degradation of Cellulose Acetate-Based Materials: A Review. J Polym Environ 19(1):152–165. https://doi.org/10.1007/s10924-010-0258-0

Robertson BP, Calabrese MA (2022) Evaporation-controlled dripping-onto-substrate (DoS) extensional rheology of viscoelastic polymer solutions. Sci Rep 12(1):4697. https://doi.org/10.1038/s41598-022-08448-x

Rochman CM, Kross SM, Armstrong JB, et al (2015) Scientific Evidence Supports a Ban on Microbeads. Environ Sci Tech 49(18):10,759–10,761. https://doi.org/10.1021/acs.est.5b03909

Rodriguez F, Patel SK, Cohen C (1990) Measuring the modulus of a sphere by squeezing between parallel plates. J Appl Polym Sci 40(1-2):285–295. https://doi.org/10.1002/app.1990.070400122

Sameni J, Krigstin S, Jaffer SA, et al (2018) Preparation and characterization of biobased microspheres from lignin sources. Ind Crops Prod 117:58–65

SAPEA (2019) Science Advice for Policy by European Academies. SAPEA Berlin, Germany

Schmalbach KM, Lin AC, Bufford DC, et al (2021) Nanomechanical mapping and strain rate sensitivity of microcrystalline cellulose. J Mater Res 36(11):2251–2265.

https://doi.org/10.1557/s43578-021-00138-0

Shareef MY, Shareef FMY (2021) Determination of Microbeads from Paste in Some Pharmaceuticals and Personal Care Products. Pharm Sci Technol 5(2):53. https://doi.org/10.11648/j.pst.20210502.15

Sipe JM, Bossa N, Berger W, et al (2022a) From bottle to microplastics: Can we estimate how our plastic products are breaking down? Sci Total Environ 814:152,460

Sipe JM, Bossa N, Berger W, et al (2022b) From bottle to microplastics: Can we estimate how our plastic products are breaking down? Science of The Total Environment 814:152,460. https://doi.org/10.1016/j.scitotenv.2021.152460

Søgaard K, Laursen B, Jensen BR, et al (2001) Dynamic loads on the upper extremities during two different floor cleaning methods. Clin Biomech 16(10):866–879. https://doi.org/10.1016/S0268-0033(01)00083-3

Tan X, Chen L, Li X, et al (2019) Effect of anti-solvents on the characteristics of regenerated cellulose from 1-ethyl-3-methylimidazolium acetate ionic liquid. International Journal of Biological Macromolecules 124:314–320. https://doi.org/10.1016/j.ijbiomac.2018.11.138

Trygg J, Fardim P, Gericke M, et al (2013) Physicochemical design of the morphology and ultrastructure of cellulose beads. Carbohydr Polym 93(1):291–299. https://doi.org/10.1016/j.carbpol.2012.03.085

Usman S, Abdull Razis AF, Shaari K, et al (2022) The Burden of Microplastics Pollution and Contending Policies and Regulations. Int J Environ Res Public Health 19(11):6773. https://doi.org/10.3390/ijerph19116773

Volant C, Balnois E, Vignaud G, et al (2021) Design of Polyhydroxyalkanoate (PHA) Microbeads with Tunable Functional Properties and High Biodegradability in Seawater. J Polym Environ https://doi.org/10.1007/s10924-021-02345-6

Xanthos D, Walker TR (2017) International policies to reduce plastic marine pollution from single-use plastics (plastic bags and microbeads): A review. Mar Pollut Bull 118(1):17–26. https://doi.org/10.1016/j.marpolbul.2017.02.048

Xia Y, Li X, Yuan Y, et al (2022) Preparation of cellulose beads with high homogeneity, low crystallinity, and tunable internal structure. Cellulose 29(3):1473–1485. https://doi.org/10.1007/s10570-021-04413-5

Xu C, Gerling GJ (2020) Time-dependent Cues Encode the Minimum Exploration Time in Discriminating Naturalistic Compliances. In: 2020 IEEE Haptics Symposium (HAPTICS), pp 22–27, https://doi.org/10.1109/HAPTICS45997.2020.ras.HAP20.7.ec43f6a7

Xu C, Hauser SC, Wang Y, et al (2019) Roles of Force Cues and Proprioceptive Joint Angles in Active Exploration of Compliant Objects. In: 2019 IEEE World Haptics Conference (WHC), pp 353–358, https://doi.org/10.1109/WHC.2019.8816159

Yurtsever M, Yurtsever U (2019) Use of a convolutional neural network for the classification of microbeads in urban wastewater. Chemosphere 216:271–280. https://doi.org/10.1016/j.chemosphere.2018.10.084

Zervos S (2010) Natural and accelerated ageing of cellulose and paper: A literature review. Cellulose: structure and properties, derivatives and industrial uses pp 155–203

Zhang DY, Calabrese MA (2022) Temperature-controlled dripping-onto-substrate (dos) extensional rheometry of polymer micelle solutions. Soft Matter 18:3993 – 4008. URL http://www.doi.org/10.1039/d2sm00377e

Zhang M, Guo W, Ren M, et al (2020) Fabrication of porous cellulose microspheres with controllable structures by microfluidic and flash freezing method. Mater Lett 262:127,193. https://doi.org/10.1016/j.matlet.2019.127193

Zhao W, Simmons B, Singh S, et al (2016) From lignin association to nano-/microparticle preparation: extracting higher value of lignin. Green Chem 18(21):5693–5700

Ziajahromi S, Neale PA, Rintoul L, et al (2017) Wastewater treatment plants as a pathway for microplastics: Development of a new approach to sample wastewater-based microplastics. Water Res 112:93–99. https://doi.org/10.1016/j.watres.2017.01.042